Nature Communications

https://doi.org/10.1038/s41467-025-68268-1

Article in Press

Cycloreversion-enhanced toughness and degradability in mechanophore-embedded end-linked polymer networks

Received: 21 May 2025

Accepted: 24 December 2025

Cite this article as: Li, Z., Tang, S. Cycloreversion-enhanced toughness and degradability in mechanophore-embedded end-linked polymer networks. *Nat Commun* (2025). https://doi.org/10.1038/s41467-025-68268-1

Zhuang Li & Shan Tang

Cycloreversion-enhanced toughness and degradability in mechanophore-embedded end-linked polymer networks

Zhuang Li[1], and Shan Tang*[1]

[1]Frontiers Science Center for Transformative Molecules, Shanghai Key Laboratory for Molecular Engineering of Chiral Drugs, School of Chemistry and Chemical Engineering, Shanghai Jiao Tong University, Shanghai 200240, China.
*Corresponding author, Email: tang.shan@sjtu.edu.cn.

ABSTRACT: Enhancing the toughness while achieving triggerable degradation in single-network polymer systems without modifying their inherent chemical composition or network architecture remains a significant challenge. Here we demonstrate a smart end-linked polymer network that "self-strengthen" during use yet "self-destruct" upon certain stimuli. Embedding nonscissile cyclobutane-fused tetrahydrofuran mechanophores within the middle of end-linked polymer networks significantly enhances both toughness and degradability. Under mechanical stress, the force-coupled cycloreversion of these mechanophores releases concealed chain segments, enabling single-network materials to exhibit threefold toughness and tenfold tear energies compared to conventional counterparts. Additionally, ball-milling griding of the bulk material unveils acid-sensitive enol ether units, leading to a markedly improved degradation profile under acidic conditions. This dual effect—originating from the force-coupled cycloreversion of cyclobutane-fused tetrahydrofuran mechanophores—provides an ideal combination of superior mechanical performance and on-demand degradability.

Introduction

As crosslinked polymer networks become increasingly prevalent in biomedical devices and flexible electronics,[1,2] there is a growing demand for materials that offer both superior mechanical strength and triggerable, on-demand degradation. Polymer mechanochemistry uses mechanical force to trigger chemical reactions in polymers, offering great promise for improving material performance.[3] Recently, increasing attention has been focused on using mechanochemistry to modulate the structure and properties of polymer networks.[4,5] By integrating stress-responsive mechanophores into polymer chains, researchers can precisely control force transmission and target crack initiation. One approach is to harness the intermediates generated by force-induced bond scission to initiate chemical reactions within the material, thereby endowing the polymer networks with self-strengthening properties.[6-12] However, this approach generally alters the polymer network architecture and introduces complexities in large-scale manufacturing.

In addition to force-induced chemical transformations, toughness can be enhanced by dissipating energy through premature mechanophore activation within a polymer network. In this context, incorporating scissile mechanophores as cross-linkers in randomly cross-linked networks produces markedly tougher materials.[13,14]

During the stretching process, mechanophore cross-links act as sacrificial bonds, enabling the primary polymer strands chains to stretch rather than fracture. Moreover, embedding nonscissile cyclobutane mechanophores into the primary network of double-network hydrogels has also been shown to double their tearing energies by unveiling hidden hydrocarbon chain segments.[15] However, owing to the inherent brittleness of the primary network, this reinforcing effect only becomes apparent upon introduction of a secondary network.

Embedding scissile mechanophores such as cyclobutane derivatives into the middle of end-linked polymer networks generally yields similar swelling ratios and moduli but significantly lower fracture strains and tearing energies compared to gels without mechanophores (Fig. 1a).[16-18] In contrast to randomly cross-linked systems, premature mechanophore activation usually creates defects to weaken the materials due to the highly cross-linked architecture and brittle property of end-linked networks. Until now, conventional mechanophores have failed to enhance the toughness of end-linked polymer networks, underscoring the need for innovative mechanophore designs.[19] Inspired by the releasing hidden length effect in double-network hydrogels,[15] we therefore envision whether a bicyclic cyclobutane mechanophore might endow a highly cross-linked, single-network polymer with enhanced toughness.[20]

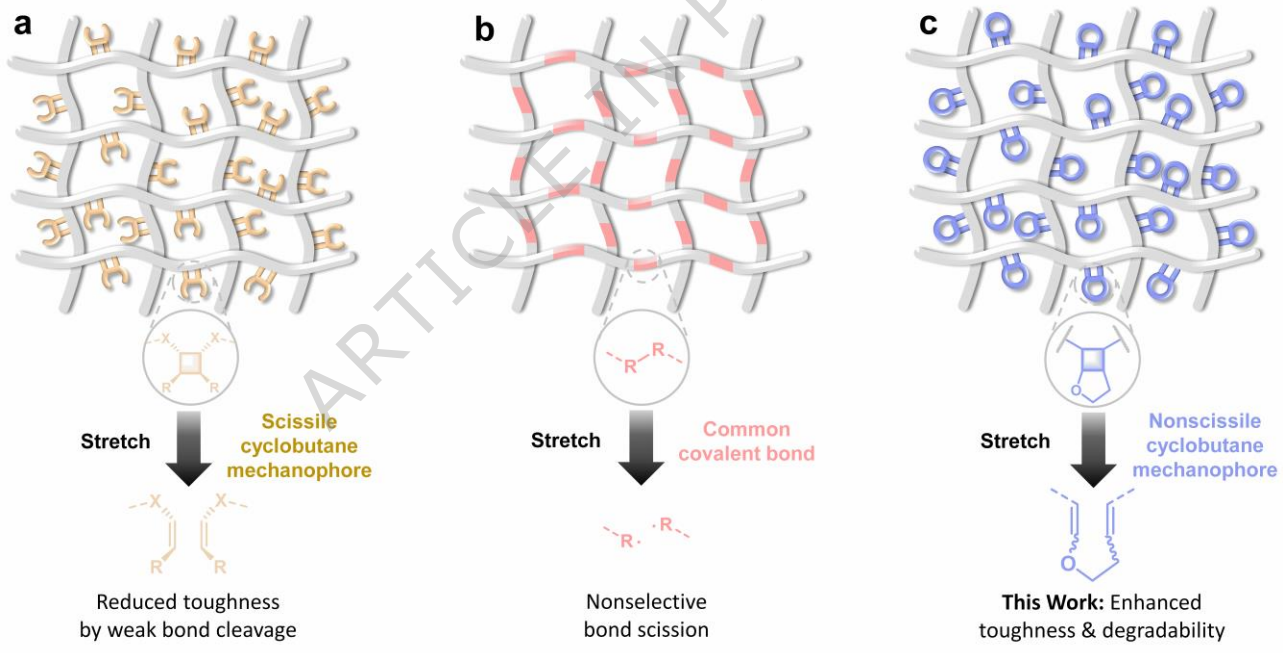

Fig. 1. Effect of different bonds on the material properties of end-linked polymer networks. a, Embedding scissile cyclobutane mechanophores. **b**, Traditional covalent bonds without mechanophores. **c**, ***This work***: embedding nonscissile cyclobutane-fused tetrahydrofuran mechanophores.

Here we demonstrate that embedding nonscissile cyclobutane-fused tetrahydrofuran mechanophores into the middle of end-linked polymer networks significantly enhances both the toughness and degradability (Fig. 1c). The dual enhancing effect is attributed to the force-coupled cycloreversion of cyclobutane-fused tetrahydrofuran

mechanophores, which released both hidden lengths and acid-sensitive enol ether units to the polymer chains.[21] Compared to the conventional analogues, embedding nonscissile cyclobutane-fused tetrahydrofuran mechanophores lead to networks that stretch 100% further and exhibit tear energies that are nine times larger. We have observed that releasing hidden lengths of nonsciccile mechanophores in highly cross-linked single-network systems enhances the strength of the materials. Notably, integration of bicyclic cyclobutane mechanophores have been reported to maintain material stability until an external force triggers degradation on demand.[21-28] In addition to the toughening effect, the incorporation of nonscissile cyclobutane-fused tetrahydrofuran mechanophores also improved the degradability when the materials were treated with ball-milling grinding under bulk conditions.[21] The unveiled enol ether units enabled the polymer network materials with significantly accelerated degradation rate under acidic conditions. Therefore, the described end-linked polymer network possesses an ideal combination of desirable mechanical properties and on-demand degradability.

Results and discussion

Photopolymerization is a fast and versatile method used in many applications—from fabricating high-resolution 3D printed objects to producing microfluidic devices.[29] Initially, we employed the well-established thiol-ene photopolymerization[30] to access end-linked polymer networks with nonscissile cyclobutane-fused tetrahydrofuran mechanophores. A diallyl ether monomer bearing a cyclobutane-fused tetrahydrofuran mechanophore (**C3**) was designed and easily synthesized from dimethyl acetylenedicarboxylate, 2,3-dihydrotetrahydrofuran and allyl bromide in large scale. Meanwhile, **C1** bearing a scissile mechanophore and **C2** without mechanophore were prepared to understand the influence of cyclobutane-fused tetrahydrofuran mechanophore on the following formed end-linked polymer networks. Since the preparation of polymer networks through step-growth polymerization requires the participation of monomers with a functional degree greater than two, a commercially available tetrafunctional monomer, pentaerythritol tetra(3-mercaptopropionate) (**PETMP**), was selected as the crosslinker. Using diphenyl(2,4,6-trimethylbenzoyl)phosphine oxide (**TPO**) as an initiator, photoinduced thiol-ene step-growth polymerization was carried out with the synthesized diene monomers (Fig. 2a). Initially, solutions of $[\mathbf{C1}]_0$:$[\mathbf{PETMP}]_0$ = 2:1 for **PN1**, $[\mathbf{C2}]_0$:$[\mathbf{PETMP}]_0$ = 2:1 for **PN2**, $[\mathbf{C2}]_0$: $[\mathbf{C3}]_0$: $[\mathbf{PETMP}]_0$ = 1:1:1 for **PN3** and $[\mathbf{C3}]_0$:$[\mathbf{PETMP}]_0$ = 2:1 for **PN4** were prepared, followed by the addition of 0.5 wt% TPO. After thorough dissolution, the mixtures were added to Teflon molds and subjected to photocuring under the irradiation of a 405 nm purple LED. Crosslinking was successfully achieved within minutes. To ensure high monomer conversion, the irradiation time was extended to one hour, resulting in complete and highly crosslinked films **PN1, PN2, PN3** and **PN4** (Supplementary Fig. 11). FTIR spectroscopy confirmed the completion of the photopolymerization process, as the characteristic absorption peaks at 1646 cm^{-1} and 2568 cm^{-1} corresponding to C=C and S–H bonds completely disappeared after the photocuring process (Supplementary Figs. 12-15). The structural similarity of **C1, C2** and **C3** led to comparable polymerization reactivity. Therefore, when resin solutions of the same

ratio were prepared, **PN1-4** with identical polymer network structures were expected to be obtained. The four polymer networks differed only in the mechanochemically responsive structural units at the bridging junctions.

To determine the influence of cyclobutane-fused tetrahydrofuran mechanophores on the strength of polymer networks, uniaxial tensile testing experiments were performed on **PN1-4**. As expected, the representative stress-strain curves of dumbbell-shaped samples of **PN1-4** exhibited marked differences. (Fig. 2b). The maximum stress value at fracture went in the order **PN1** < **PN2** < **PN3** < **PN4**, indicating that **PN3** and **PN4** had greater strength. The introduction of the cyclobutane-fused tetrahydrofuran mechanophores enhanced the tensile strength of the material, meaning that **PN4** could withstand greater external stress before reaching the breaking point. Additionally, **PN4** exhibited a higher elongation at break than **PN1-3** (33% vs. 24% vs. 19% vs. 15%) and demonstrated better ductility. Notably, the stress-strain curves revealed that **PN1-4** had similar Young's moduli of 4.6 ± 0.1 MPa, 5.3 ± 0.2 MPa, 5.1 ± 0.2 MPa and 5.0 ± 0.2 MPa, respectively (Fig. 2c). This indicated that, apart from the differences in the embedded mechanical mechanophores structures, **PN1-4** had similar crosslinking densities and network structures, showing no essential difference under stress conditions insufficient to activate the mechanophores. In comparison to **PN2** (88.2 ± 6.4 kJ/m^3), **PN1** exhibited reduced toughness (46.1 ± 0.9 kJ/m^3), whereas **PN4** demonstrated a significant increase in toughness (258.5 ± 24.1 kJ/m^3) (Fig. 2d). Polymer networks with different mechanophore contents exhibit varying levels of toughness (**PN4** > **PN3** > **PN2**), suggesting a positive correlation between toughness and the number of cyclobutane-fused tetrahydrofuran mechanophores. The difference in toughness between **PN1-4** could be attributed to distinct mechanophores at the bridging junctions. Given that the cyclobutane unit constitutes a scissile mechanophore, premature mechanophore activation usually creates defects to weaken the polymer network. However, the bicyclic structure of the cyclobutane-fused tetrahydrofuran mechanophore could dissipate part of the energy through ring cleavage and reduction under certain stress, followed by the release of the length stored in the cyclobutane structure.[15] This process promoted chain extension within the single-network materials, thereby achieving higher fracture stress and elongation at break.

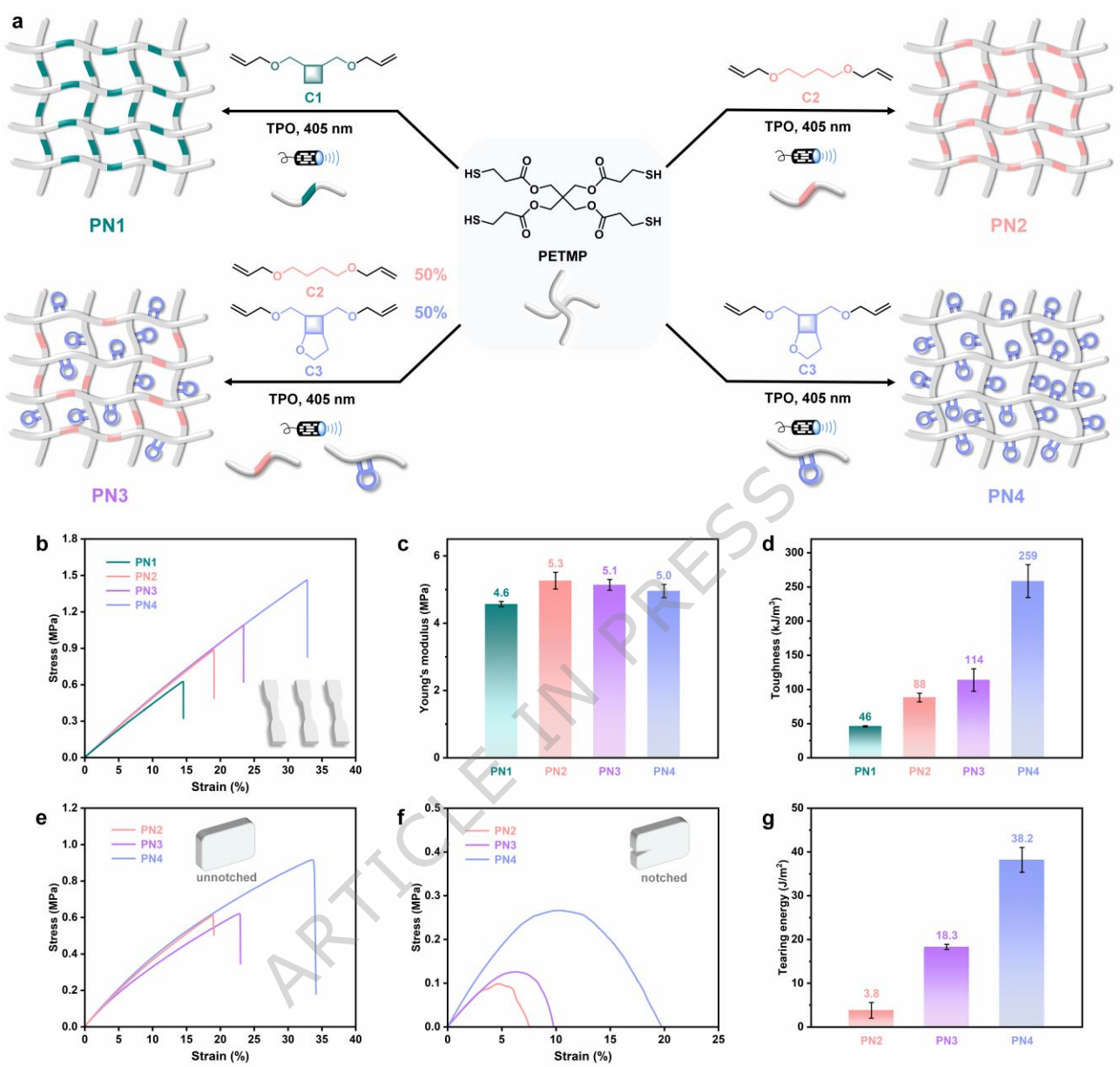

Fig. 2. Influences of cyclobutane-fused tetrahydrofuran mechanophores on the mechanical properties of end-linked polymer networks. a, General method for the preparation of **PN1-4**. **b,** Representative stress strain curves, **c**, Young's modulus (The error bars represent the standard deviation of the mean based on three samples.), and **d,** Toughness of the dumbbell shaped samples for **PN1** and **PN2** (The error bars represent the standard deviation of the mean based on three samples.). **e**, Representative stress strain curves of unnotched rectangular samples for **PN2-4**. **f**, Representative stress strain curves of notched rectangular samples for **PN2-4**. **g**, Tear energies for **PN2-4** (The error bars represent the standard deviation of the mean based on three samples.).

To further quantitatively determine the strength difference between **PN1-4**, the tear energies of **PN1-4** were characterized using the Rivlin-Thomas method for notched films in pure shear geometry.[31] Unfortunately, the inherent brittleness of **PN1** precludes reliable tear resistance characterization. The representative stress-strain curves of unnotched and notched samples for **PN2-4** under uniaxial tensile conditions are shown in Figs. 2e and

2f. The stress-strain behavior of the unnotched samples for **PN2-4** was identical before reaching the ultimate fracture point, confirming that **PN2-4** had similar polymer network structures. However, the critical stress and strain required for fracture were both lower for **PN2** than for **PN3** and **PN4**, indicating that **PN3** and **PN4** exhibit superior toughness compared to **PN2**. Although these polymer networks had similar network structures, the introduction of the cyclobutane-fused tetrahydrofuran mechanophores in **PN4** led to significant changes in the tear resistance of the material. The representative stress-strain curves under uniaxial tension of the notched samples for **PN2-4** are shown in Fig. 2f, and the stress-strain behavior of notched **PN2-4** was highly reproducible (Supplementary Fig. 22). The critical tensile strain for crack growth in **PN4** was 7.9 ± 0.3%, which was greater than the observed critical tensile strain of 2.4 ± 0.6% for **PN2** and 5.7 ± 0.1% for **PN3** (Supplementary Table 2). The tear energies of **PN2-4** were determined from the critical strain required for crack growth in the notched samples, yielding values of 3.8 ± 1.8 J/m^2, 18.3 ± 0.6 J/m^2 and 38.2 ± 2.8 J/m^2, respectively (Fig. 2g). The tear energy of **PN4** was ten-fold compared to **PN2**, demonstrating that the introduction of the cyclobutane-fused tetrahydrofuran mechanophores into the end-linked polymer network significantly improved the tear energy, resulting in a tougher material.

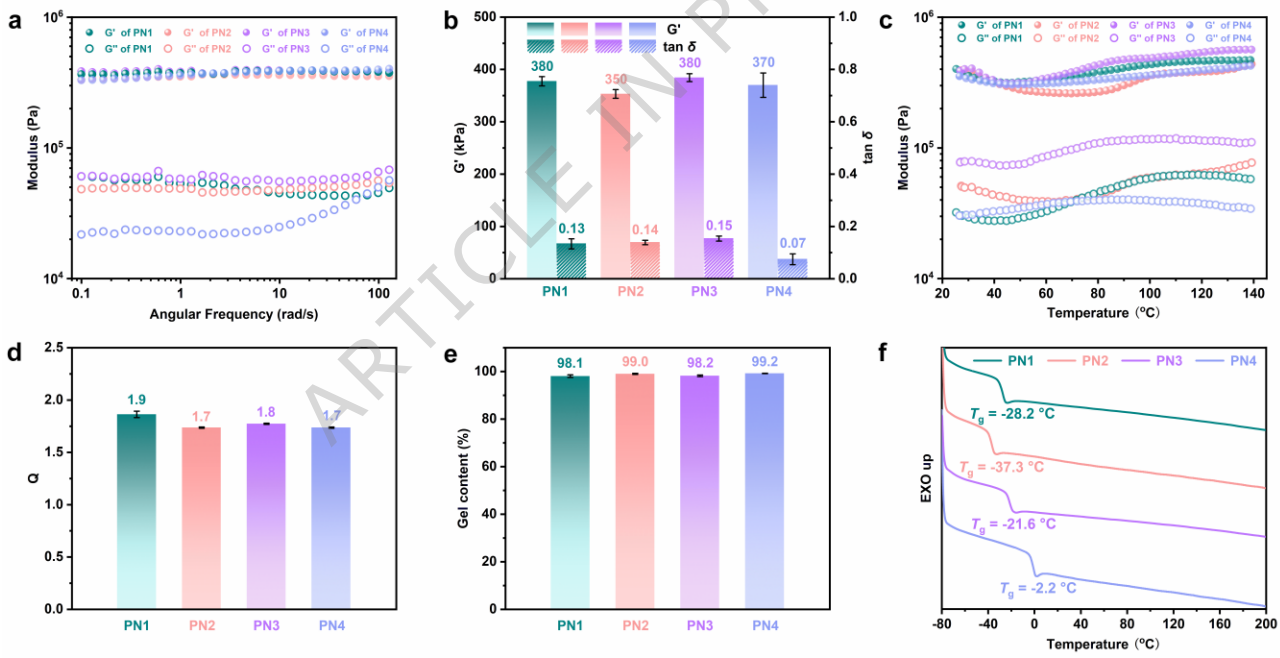

Fig. 3. **Characterization of PN1-4. a**, Rheological frequency sweeps (oscillatory strain at 1%). **b**, Storage moduli and tan δ (The error bars represent the standard deviation of the mean based on measurements across angular frequencies on a single sample.). **c**, Rheological temperature sweeps (oscillatory strain at 1%). **d**, Swelling ratios (The error bars represent the standard deviation of the mean based on three samples.). **e**, Gel contents (The error bars represent the standard deviation of the mean based on three samples.). **f**, DSC traces.

Subsequently, the shear modulus and viscoelastic properties of polymer networks were characterized using small-amplitude oscillatory rheology tests. Frequency sweep rheology from 0.1 to 100 rad/s at 25 °C and 1% strain showed that **PN1-4** exhibited similar storage moduli (G') of 380 ± 9 kPa, 353 ± 8 kPa, 380 ± 8 kPa and 370 ± 23 kPa, respectively, and G' was markedly higher than the loss modulus (G''), as evidenced by a loss factor (tan δ) < 1 (Figs. 3a and 3b), indicating that both polymer networks exhibited good and stable elastic behavior. Additionally, temperature sweep rheology from 25 °C to 140 °C at 1% strain revealed that the G' and G'' values of **PN1-4** were relatively stable, while G' values were consistently higher than G'' values, indicating that the polymer networks retain excellent elasticity and thermomechanical stability (Fig. 3c). As expected, the following consistent features were observed across **PN1-4**: (i) similar shear moduli, with nearly identical trends in G' as a function of frequency or temperature; (ii) similar swelling ratios (Fig. 3d); (iii) similar gel contents (Fig. 3e). These results further confirmed that apart from the differences in the embedded mechanophores structures, **PN1-4** possessed similar network structures. Moreover, the glass transition temperature (T_g) of **PN1-4** exhibited a range of values (Fig. 3f). The scissile cyclobutane and nonscissile cyclobutane-fused tetrahydrofuran, which have a strained ring structure, likely made the polymer chains stiffer and limited their movement, which in turn increased T_g.

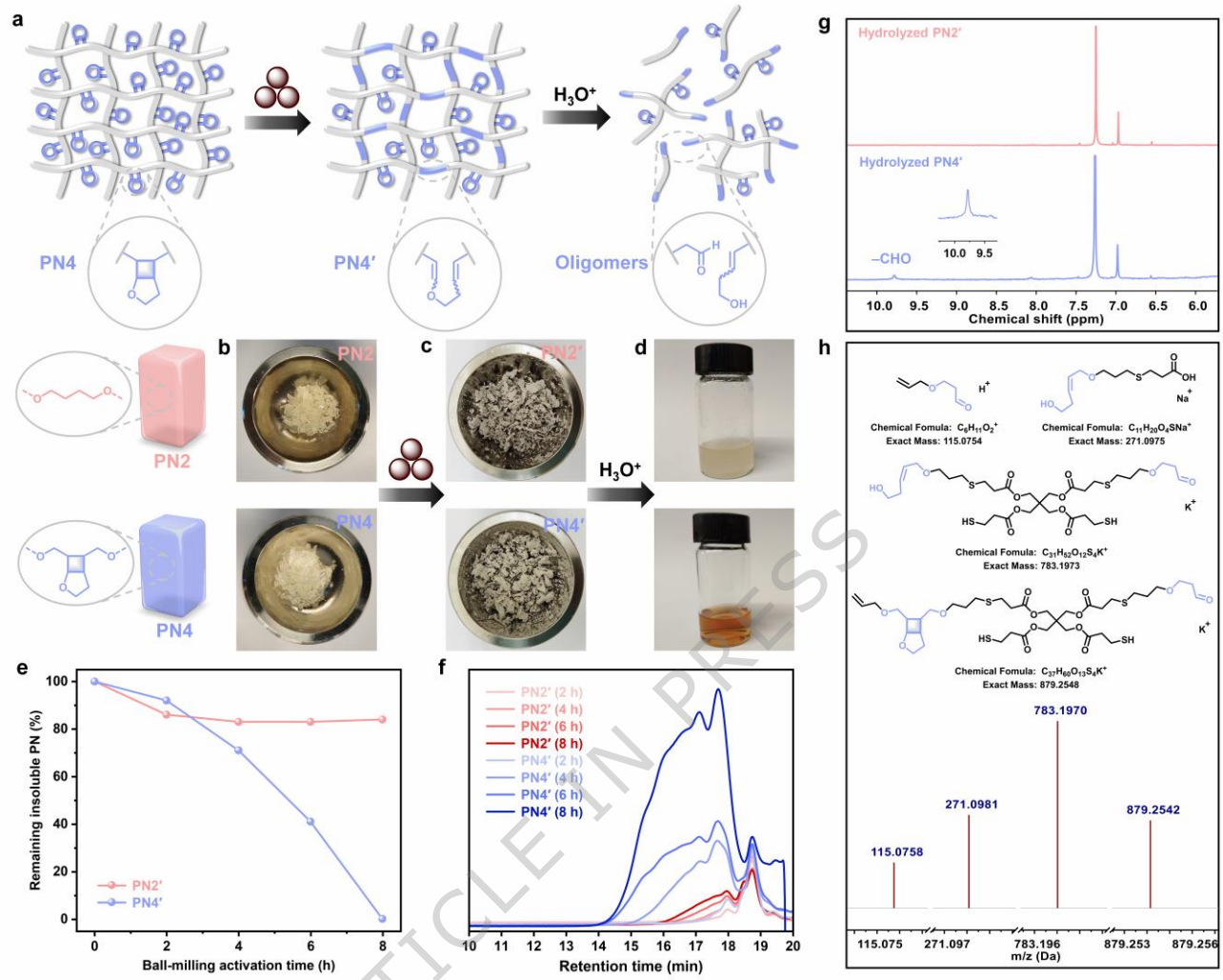

Fig. 4. **Ball-milling activation and degradation. a**, General method for chemical degradation of **PN4**. **b**, Photographs of **PN2** (top) and **PN4** (bottom) before ball-milling. **c**, Photographs of **PN2′** and **PN4′** obtained after ball-milling. **d**, Photographs of **PN2′** and **PN4′** after hydrolysis. **e**, Quantitative analysis of remaining insoluble PNs of **PN2′** and **PN4′** after acid hydrolysis at different ball-milling activation times. **f**, SEC traces of **PN2′** and **PN4′** after acid hydrolysis at different ball-milling activation times (THF, 35 °C). **g**, ^{1}H NMR spectra of **PN2′** and **PN4′** before and after hydrolysis ($CDCl_3$). **h**, HR-ESI-MS of **PN4′** after hydrolysis.

Polymer networks are known to have poor solubility in organic solvents, making their degradation particularly challenging.[32] Until now, it remains unclear how incorporating cyclobutane-fused mechanophores will influence the degradability of highly cross-linked polymer networks.[33] The introduction of the cyclobutane-fused tetrahydrofuran mechanophores not only enhanced the toughness of the polymer network through chain extension but also introduced acid-sensitive enol ether units into the main chain after the force-induced cycloreversion, effectively promoting its acid degradation (Fig. 4a). To verify the feasibility of bulk mechanical activation and acid degradation of the end-linked polymer networks, ball-milling activation experiments were conducted on the films **PN2** (Fig. 4b, top) and **PN4** (Fig. 4b, bottom). After 8 hours of ball-milling at 50 Hz under room

temperature, the morphology of the films changed significantly, resulting in light gray solids (Fig. 4c). Since both **PN2′** and **PN4′** obtained after ball-milling grinding were insoluble in THF (Supplementary Fig. 29), the size exclusion chromatography (SEC) elution curves showed low signal intensity under the premise of ensuring the same concentration of tested samples (Supplementary Fig. 30, red and blue lines). When the ball-milled materials were added to a TFA/H_2O (10/1 v/v) solution at room temperature, **PN4′** produced a clear and transparent solution within 10 minutes (Fig. 4d, bottom), while **PN2′** remained a turbid solution (Fig. 4d, top). Notably, the SEC elution curve of hydrolyzed **PN4′** displays a pronounced oligomer peak in the low molecular weight region, indicative of nearly complete hydrolysis (Supplementary Fig. 30, green line). In contrast, the SEC elution curve of hydrolyzed **PN2′** shows a much smaller oligomer peak, likely due to partial hydrolysis of the ester groups in the PETMP crosslinkers under acidic conditions (Supplementary Fig. 30, orange line).

To more clearly illustrate the difference in degradability, we quantified the insoluble solid residues and soluble small-molecule products obtained after ball-milling activation and subsequent acid hydrolysis of **PN2′** and **PN4′**. **PN2′** showed only a slight decrease in insoluble content, whereas **PN4′** exhibited a dramatic reduction (Fig. 4e). After 8 hours of ball milling, hydrolysis of **PN4′** produced completely soluble small molecules or oligomers, while approximately 80% of **PN2′** remained insoluble. Meanwhile, SEC analysis of soluble products obtained from acid hydrolysis of **PN2′** and **PN4′** (Fig. 4f) revealed that the SEC profile of hydrolyzed **PN2′** changed minimally with activation time, whereas that of hydrolyzed **PN4′** developed a strong oligomer peak in the low molecular weight region. Different from that of hydrolyzed **PN2′**, the ^{1}H NMR spectrum of the acid degradation products of **PN4′** showed a characteristic peak at 9.8 ppm, indicating the formation of aldehydes after hydrolysis (Fig. 4g). Furthermore, high resolution electrospray ionization mass spectrometry (HR-ESI-MS) analysis of the small-molecule products from **PN4′** identified the species originating from acid-hydrolyzed enol ethers (Fig. 4h). These findings confirmed that the cycloreversion of the cyclobutane-fused tetrahydrofuran mechanophores through ball-milling activation, thereby providing direct evidence for mechanophore activation. Control experiments, where **PN2** and **PN4** were not subjected to ball-milling activation, showed no oligomer formation via SEC analysis (Supplementary Fig. 34). These results demonstrate that the cyclobutane-fused tetrahydrofuran mechanophores undergo cycloreversion to form enol ethers after ball-milling, significantly enhancing the degradability of the end-linked polymer network.

In summary, we have demonstrated the dual role of nonscissile cyclobutane-fused tetrahydrofuran mechanophores in enhancing toughness while enabling triggerable degradation in single-network materials. This dual effect stems from the force-coupled cycloreversion of the mechanophores, which releases hidden lengths and acid-sensitive enol ether units within the polymer chains. Compared to conventional analogues, end-lined polymer networks incorporating these mechanophores exhibit threefold toughness and tenfold tear energies. Furthermore, the cyclobutane-fused tetrahydrofuran mechanophores also retain the elasticity and thermomechanical properties of the materials. Additionally, the incorporation of nonscissile cyclobutane-fused tetrahydrofuran mechanophores improves the degradability of the materials when subjected to ball-milling grinding under bulk

conditions. Upon ball-milling, the cycloreversion of the cyclobutane-fused tetrahydrofuran mechanophores generates acid-sensitive enol ether units, which significantly accelerate the hydrolytic degradation of the polymer network under acidic conditions. Therefore, the described end-linked polymer network with nonscissile cyclobutane-fused tetrahydrofuran mechanophores offers an ideal combination of desirable mechanical properties and on-demand degradability.

Methods

Materials. All of the commercially available reagents were used as received, unless otherwise noted. 2,3-dihydrofuran, *N*,*N*-diisopropylethylamine, 3-oxabicyclo[3.2.0]heptane-2,4-dione, allyl bromide and trifluoroacetic acid, sodium hydroxide and sodium sulfate (Na_2SO_4) were purchased from Shanghai Titan Scientific Co., Ltd.. Dimethyl acetylenedicarboxylate, palladium on activated carbon (10%, wetted with ca. 55% Water), tetrabutylammonium iodide and 1,4-butanediol were purchased from Bidepharm Co., Ltd.. Lithium aluminium hydride ($LiAlH_4$, 2.5 mol/L in THF) was purchased from Energy Chemical Co., Ltd.. Pentaerythritol tetra(3-mercaptopropionate) (PETMP) was purchased from Shanghai Aladdin Biochemical Technology Co., Ltd.. Diphenyl(2,4,6-trimethylbenzoyl)phosphine oxide (TPO) was purchased from TCI Shanghai Chemical Industrial Development Co., Ltd.. Hydrogen (H_2) was purchased from Shanghai Pujiang Special Gas Co., Ltd.. Ethyl acetate (EtOAc) and petroleum ether (PE) were purchased from Sinopharm Chemical Reagent Co., Ltd.. Toluene (Sinopham Chemical Reagent Co., Ltd.) and tetrahydrofuran (THF, J&K Scientific Co., Ltd.) were dried over Vigor VG-P7 solvent purification system under an argon atmosphere.

Nuclear magnetic resonance. Nuclear magnetic resonance spectra were recorded on Bruker Ascend 500 (^{1}H: 500 MHz, ^{13}C: 126 MHz) NMR spectrometers at ambient temperature unless otherwise noted. Chemical shift values for protons are referenced to the residual proton resonance of chloroform-*d* ($CDCl_3$-*d*: 7.26 ppm). Chemical shift values for carbons are referenced to the carbon resonances of $CDCl_3$-*d* (δ: 77.0 ppm). NMR assignments were assisted by ^{1}H-^{13}C HSQC and ^{1}H-^{13}C HMBC data.

Size exclusion chromatography. Size exclusion chromatography was performed at 35 °C with THF as mobile phase at a flow rate of 1.0 mL/min, using an Agilent 1260 Infinity LC system. The system was equipped with a PL1110-1520 guard column (PLgel 5 um Guard 50 x 7.5 mm) and two PL1110-6500 columns (PLgel 5 um MIXED-C 300 x 7.5 mm within molecular weight of 200-2,000,000 g/mol) connected in series and fitted with a 1260 infinity II Refractive Index detector. Determination of molecular weights and polydispersities were calibrated against polystyrene standards.

Differential scanning calorimetry. Differential scanning calorimetry measurements of polymers were performed on a DSC250 analyzer at a heating and cooling rate of 10 °C/min. Glass transition temperature (T_g) values were determined from the second heating scan.

Photocuring procedures. Mixtures were prepared in brown vials according to the following molar ratios: [**C1**]$_0$:[PETMP]$_0$ = 2:1 for **PN1**, [**C2**]$_0$:[PETMP]$_0$ = 2:1 for **PN2**, [**C2**]$_0$: [**C3**]$_0$: [PETMP]$_0$ = 1:1:1 for **PN3** and [**C3**]$_0$:[PETMP]$_0$ = 2:1 for **PN4**, followed by the addition of 0.5 wt% TPO to each mixture. The mixture was heated on a hot plate to accelerate dissolution and then vortexed mixing for a few seconds. The film samples (a

length of 60 mm, a width of 60 mm and a thickness of 1 mm) were prepared by adding the uniformly mixed solution into a Teflon mold and irradiated with a purple LED light (λ_{max} = 405 nm, 35 W) for one hour at 25 °C. Upon completion of photocuring procedures, the film samples were stored under light-shielded conditions in preparation for subsequent FTIR-ATR, swelling ratio, gel content, thermal and mechanical characterizations.

Fourier-transform infrared attenuated total reflectance. Fourier-transform infrared attenuated total reflectance measurements were performed on a Thermo Fisher Nicolet iS50.

Rheology. Rheological frequency sweep and temperature sweep experiments were performed on a HAAKE MARS 60 rheometer. A parallel-plate geometry with a radius of 10 mm was used and coupled with a bottom plate, maintaining a typical gap between 1.00-1.15 mm. Frequency sweep experiments were conducted from 0.1 to 100 rad/s with a constant oscillatory strain of 1% at 25 °C. Temperature sweep experiments were conducted at a heating rate of 5 °C/min with a constant oscillatory strain of 1%.

Tensile measurements. Tensile measurements were conducted on an Instron 3343 machine testing instrument at ambient conditions (25 °C). Upon completion of photocuring procedures, the film samples were carefully demolded and subsequently sectioned into dumbbell-shaped samples (a length of 35 mm, a width of 6 mm and a thickness of 1 mm) using a custom-designed die-cutting apparatus. Tensile measurements were conducted on an Instron 3343 machine testing instrument at ambient conditions, stretched at 2.4 mm/min until fracture. Young's modulus was calculated as the slope of the stress-strain curve within the strain range of 0% to 1%. Toughness was calculated by integrating the stress strain curves up to the point of fracture.

Tearing energy. Tearing energy measurements were coducted using the Rivlin-Thomas method. Upon completion of photocuring procedures, the film samples were carefully demolded and subsequently sectioned into several rectangular samples (a length of 20 mm, a width of 16 mm and a thickness of 1 mm) using a razor blade. For notched rectangular samples, a 5 mm notch was introduced in the center of one side of the rectangle using a razor blade, perpendicular to the edge. Tearing energy measurements were conducted on an Instron 3343 machine testing instrument at ambient conditions, using the pure shear geometry with both notched and unnotched rectangular samples. The notched and unnotched rectangular samples were put into the tensile grips with a gauge length of 3 mm and then stretched at 0.66 mm/min until fracture. Tearing energy ($\boldsymbol{\Gamma}$) was calculated by integrating unnotched stress-strain curves up to the critical strain ($\boldsymbol{\varepsilon_p}$) at which the crack of the notched samples began to propagate to determine strain energy density $\boldsymbol{W(\varepsilon_p)}$ and then multiplying by the sample gauge length ($\boldsymbol{h_0}$).

$$\boldsymbol{\Gamma = W(\varepsilon_p)h_0}$$

Swelling ratios and gel contents. The disc samples (×3) of **PN1-4** (10 mm diameter, 1 mm thick) were weighted and submerged in THF for 24 h, and then the mass of the swollen samples was measured. Subsequently, the samples were dried in a vacuum oven until a constant weight was achieved and the mass of the dried samples was recorded. The swelling ratios were calculated by (mass of the swollen sample)/(mass of the dry sample). The gel contents were calculated by (mass of the dry sample)/(initial mass)×100%.

Ball-milling activation and degradation experiments. Experimental procedure for the kinetic study of the ball-milling activation process: Ball-milling activation experiments were conducted using a 25 mL stainless steel

grinding jar with stainless steel grinding balls on Tissuelyser-II (Shanghai Jingxin®) with a frequency of 50 Hz. 500 mg polymer networks (**PN2** or **PN4**) were initially cut into small pieces and then placed into a 25 mL stainless steel grinding jar containing a single stainless steel grinding ball with a diameter of 20 mm. The stainless steel grinding jar with polymers was was subjected to grinding for 2 hours at a frequency of 50 Hz. Subsequently, the 20 mm grinding ball was replaced with one 14 mm stainless steel grinding ball and 50 stainless steel grinding balls, each with a diameter of 4 mm. The grinding process was then continued at the same frequency of 50 Hz for an additional 6 hours. Among them, each 30-minute ball milling period is immediately followed by a 30-minute pause, repeating in this cyclic manner. Experimental procedure for the kinetic study of the degradation process: During the ball-milling activation process, polymer network films (20 mg) were taken every two hours and dissolved in 5 mL of a 10/1 (v/v) TFA/H_2O mixture. The mixture was stirred at room temperature for 10 minutes. Subsequently, all volatile components were removed under vacuum. An appropriate amount of THF was added to dissolve the residue, followed by centrifugation to separate the insoluble fraction. The supernatant was concentrated under reduced pressure to obtain the dissolved portion (small-molecule products). After drying in a vacuum oven, both fractions were weighed separately to calculate insoluble solids contents and soluble small-molecule products contents after hydrolysis. The obtained oligomers were then redissolved in 4.5 mL of THF for SEC analysis.

High resolution electrospray ionization mass spectrometry. High resolution electrospray ionization mass spectrometry spectra were recorded on a Waters Synapt HDMS quadrupole/time-of-flight (Q-ToF) mass spectrometer (Waters, Beverly, MA) in both positive and negative ion modes.

Data availability

All the other data supporting the findings of this study are available within the article and its Supplementary Information. All data are available from the corresponding author upon request.

References

1 Root, S. E., Savagatrup, S., Printz, A. D., Rodriquez, D. & Lipomi, D. J. Mechanical Properties of Organic Semiconductors for Stretchable, Highly Flexible, and Mechanically Robust Electronics. *Chem. Rev.* **117**, 6467-6499, (2017).

2 Zhao, X. *et al.* Soft Materials by Design: Unconventional Polymer Networks Give Extreme Properties. *Chem. Rev.* **121**, 4309-4372, (2021).

3 Caruso, M. M. *et al.* Mechanically-Induced Chemical Changes in Polymeric Materials. *Chem. Rev.* **109**, 5755-5798, (2009).

4 Lloyd, E. M., Vakil, J. R., Yao, Y., Sottos, N. R. & Craig, S. L. Covalent Mechanochemistry and Contemporary Polymer Network Chemistry: A Marriage in the Making. *J. Am. Chem. Soc.* **145**, 751-768, (2023).

5 Wang, Z. J. & Gong, J. P. Mechanochemistry for On-Demand Polymer Network Materials. *Macromolecules* **58**, 4-17, (2025).

6 Ramirez, A. L. B. *et al.* Mechanochemical strengthening of a synthetic polymer in response to typically destructive shear forces. *Nat. Chem.* **5**, 757-761, (2013).

7 Zhang, H. *et al.* Mechanochromism and Mechanical-Force-Triggered Cross-Linking from a Single Reactive Moiety Incorporated into Polymer Chains. *Angew. Chem. Int. Ed.* **55**, 3040-3044, (2016).

8 Pan, Y. *et al.* A Mechanochemical Reaction Cascade for Controlling Load-Strengthening of a Mechanochromic Polymer. *Angew. Chem. Int. Ed.* **59**, 21980-21985, (2020).

9 Seshimo, K. *et al.* Segmented Polyurethane Elastomers with Mechanochromic and Self-Strengthening Functions. *Angew. Chem. Int. Ed.* **60**, 8406-8409, (2021).

10 Zheng, Y. *et al.* In Situ and Real-Time Visualization of Mechanochemical Damage in Double-Network Hydrogels by Prefluorescent Probe via Oxygen-Relayed Radical Trapping. *J. Am. Chem. Soc.* **145**, 7376-7389, (2023).
11 Wang, Z. J. *et al.* Rapid self-strengthening in double-network hydrogels triggered by bond scission. *Nat. Mater.*, **24**, 607-614, (2025).
12 Li, X. *et al.* Weak Covalent Bonds and Mechanochemistry for Synergistic Self-Strengthening of Elastomers. *J. Am. Chem. Soc.* **147**, 4357-4364, (2025).
13 Wang, S. *et al.* Facile mechanochemical cycloreversion of polymer cross-linkers enhances tear resistance. *Science* **380**, 1248-1252, (2023).
14 Yokochi, H. *et al.* Sacrificial Mechanical Bond is as Effective as a Sacrificial Covalent Bond in Increasing Cross-Linked Polymer Toughness. *J. Am. Chem. Soc.* **145**, 23794-23801, (2023).
15 Wang, Z. *et al.* Toughening hydrogels through force-triggered chemical reactions that lengthen polymer strands. *Science* **374**, 193-196, (2021).
16 Wang, S. *et al.* Mechanism Dictates Mechanics: A Molecular Substituent Effect in the Macroscopic Fracture of a Covalent Polymer Network. *J. Am. Chem. Soc.* **143**, 3714-3718, (2021).
17 Li, Y. *et al.* Azobenzene as a photoswitchable mechanophore. *Nat. Chem.* **16**, 446-455, (2024).
18 Beech, H. K. *et al.* Reactivity-Guided Depercolation Processes Determine Fracture Behavior in End-Linked Polymer Networks. *ACS Macro Lett.* **12**, 1685-1691, (2023).
19 Herzog-Arbeitman, A. *et al.* Tetrafunctional cyclobutanes tune toughness via network strand continuity. *Nat. Chem.*, doi: 10.1038/s41557-025-01984-9, (2025).
20 Zheng, X. *et al.* Tuning the Ultimate Strain of Single and Double Network Gels Through Reactive Strand Extension. *ACS Cent. Sci.* **11**, 1882-1891, (2025).
21 Yang, J. & Xia, Y. Mechanochemical generation of acid-degradable poly(enol ether)s. *Chem. Sci.* **12**, 4389-4394, (2021).
22 Lin, Y., Kouznetsova, T. B. & Craig, S. L. Mechanically Gated Degradable Polymers. *J. Am. Chem. Soc.* **142**, 2105-2109, (2020).
23 Hsu, T.-G. *et al.* A Polymer with "Locked" Degradability: Superior Backbone Stability and Accessible Degradability Enabled by Mechanophore Installation. *J. Am. Chem. Soc.* **142**, 2100-2104, (2020).
24 Lin, Y., Kouznetsova, T. B., Chang, C.-C. & Craig, S. L. Enhanced polymer mechanical degradation through mechanochemically unveiled lactonization. *Nat. Commun.* **11**, 4987, (2020).
25 Hsu, T.-G. *et al.* Mechanochemically accessing a challenging-to-synthesize depolymerizable polymer. *Nat. Commun.* **14**, 225, (2023).
26 Liu, P. *et al.* Mechanically triggered on-demand degradation of polymers synthesized by radical polymerizations. *Nat. Chem.* **16**, 1184–1192, (2024).
27 Li, Z., Zhang, X., Zhao, Y. & Tang, S. Mechanochemical Backbone Editing for Controlled Degradation of Vinyl Polymers. *Angew. Chem. Int. Ed.* **63**, e202408225, (2024).
28 Zhang, X. *et al.* Polyethylene Materials with Tunable Degradability by Incorporating In-Chain Mechanophores. *J. Am. Chem. Soc.* **146**, 24024-24032, (2024).
29 Bagheri, A. & Jin, J. Photopolymerization in 3D Printing. *ACS Appl. Polym. Mater.* **1**, 593-611, (2019).
30 Hoyle, C. E. & Bowman, C. N. Thiol–Ene Click Chemistry. *Angew. Chem. Int. Ed.* **49**, 1540-1573, (2010).
31 Rivlin, R. S. & Thomas, A. G. Rupture of rubber. I. Characteristic energy for tearing. *J. Polym. Sci.* **10**, 291-318, (2003).
32 Fortman, D. J. *et al.* Approaches to Sustainable and Continually Recyclable Cross-Linked Polymers. *ACS Sustainable Chem. Eng.* **6**, 11145-11159, (2018).
33 Rajasooriya, T., Ogasawara, H., Dong, Y., Mancuso, J. N. & Salaita, K. Force-Triggered Self-Destructive Hydrogels. *Adv. Mater.* **35**, 2305544, (2023).

Acknowledgements

This research was supported by the National Natural Science Foundation of China (52473097), and the Fundamental Research Funds for the Central Universities (25X010202131, 24X010301678). We thank Prof. G. Tong (SJTU) for the help with FTIR-ATR and rheological measurements, Prof. X. Yan (SJTU) for the technical help with tensile strength measurements.

Author contributions

S.T. contributed to the conception and design of the experiments. Z.L. performed the experiments. S.T. and Z.L. cowrote the manuscript, and S.T. directed the project.

Competing interests

The authors declare no competing financial interests or any non-financial competing interests.

Editorial Summary:

Achieving both high toughness and degradability in mechanophore containing polymer networks is a challenge. Here, the authors incorporated non-scissile cyclobutane-fused tetrahydrofuran mechanophores into end-linked polymer networks to enhance their toughness and degradability through mechanically triggered cycloreversion reactions.

Peer review information: *Nature Communications* thanks the anonymous reviewers for their contribution to the peer review of this work. A peer review file is available.